TABLE I
VOLTAGE VECTORS

Vector	Switching Symbol		NP Current		Proportion(Vx/Vdc)
Zero Vector	(PPP),(OOO),(NNN)		0		0
Small Vector	P-Type	N-Type	P-Type	N-Type	$\frac{1}{3}$
	[POO]	[ONN]	-Ia	Ia	
	[PPO]	[OON]	Ic	-Ic	
	[OPO]	[NON]	-Ib	Ib	
	[OPP]	[NOO]	Ia	-Ia	
	[POP]	[ONO]	Ib	-Ib	
	[OOP]	[NNO]	-Ic	Ic	
Medium Vector	[PON]		Ib		$\frac{\sqrt{3}}{3}$
	[OPN]		Ia		
	[NPO]		Ic		
	[NOP]		Ib		
	[ONP]		Ia		
	[PNO]		Ic		
Large Vector	[PNN]		-		$\frac{2}{3}$
	[PPN]		-		
	[NPN]		-		
	[NPP]		-		
	[NNP]		-		
	[PNP]		-		

$$\begin{cases} \vec{V}_{obj}T = \vec{V}_{PON}T_{ori} \\ \vec{V}_{obj}T = (\vec{V}_{OON} + \vec{V}_{PPO} + \vec{V}_{PON})T_v/3 \end{cases} \quad (9)$$

where T_{ori} is the time for the original one, and T_v is the time for the virtual one. The result of Equ. (9) is $T_v = 1.5T_{ori}$, which means that the virtual medium vector needs a longer time than the original one to synthesize the same reference vector.

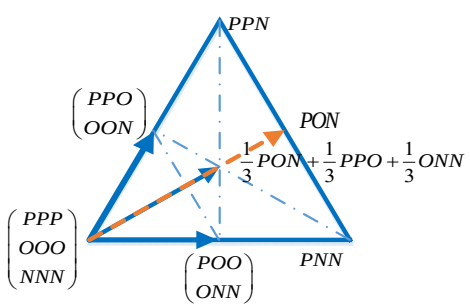

Fig. 3. Vectors in Sector III.

Considering that the vectors are applied in one switching period, a long time for the virtual medium vector means the time for virtual small vectors is compressed. In addition, the time used to regulate the NPP is decreased. When the NPP drifts in a high MI, the regulation process is lengthened. To cope with this issue, an improved strategy is presented in next section.

III. THE PROPOSED MODULATION METHOD

In Section I, it was briefed that the FCS-MPC is suitable to regulate the NPP. The detail of it is presented in this section. First, the two-step discrete model for the FCS-MPC is presented in this section. Second, the relationship between the MMV and the model predictive algorithm is analysed.

A. The MPC Algorithm

The FCS-MPC utilizes discrete voltage vectors as the elements to implement the optimal research. Its steps are as follows:

1) Construct a mathematical model of the system.
2) Transfer this model into the discrete time domain.
3) Based on the control object, formulate the cost function.
4) Select vectors that minimize the cost function.

Assume that the filters in the three phases are identical. The

mathematical expressions of the inverter in the αβ axes are demonstrated,

$$\begin{cases} \frac{di_\alpha}{dt} = \frac{u_\alpha - e_\alpha - Ri_\alpha}{L} \\ \frac{di_\beta}{dt} = \frac{u_\beta - e_\beta - Ri_\beta}{L} \end{cases} \quad (10)$$

where L is the filter inductance; R is the filter resistance; u_α, u_β are the inverter's output voltage; and e_α, e_β are the load voltage.

Based on the forward Euler approximation [34], the derivative of the current is approximated to:

$$L\frac{di}{dt} \approx L\frac{i(k+1)-i(k)}{T_s} \quad (11)$$

where $i(k)$ is the current value sampled at the kth instant, and $i(k+1)$ is the predicted value at next sampling step.

Assuming the resistance is neglected, the model in the discrete time domain is:

$$\begin{cases} i_\alpha(k+1) = \frac{T_s\left[u_\alpha(k) - e_\alpha(k) - \left(1-\frac{T_s}{L}\right)i_\alpha(k)\right]}{L} \\ i_\beta(k+1) = \frac{T_s\left[u_\beta(k) - e_\beta(k) - \left(1-\frac{T_s}{L}\right)i_\beta(k)\right]}{L} \end{cases} \quad (12)$$

where $u_\alpha(k)$, $u_\beta(k)$, $e_\alpha(k)$, $e_\beta(k)$, $i_\alpha(k)$ and $i_\beta(k)$ are the initial values at the kth instant. $i_\alpha(k+1)$ and $i_\beta(k+1)$ are the predicted value at the $(k+1)th$ instant. The value of the back-EMF $e_j(k)$ is regarded as a constant during the sampling period. Therefore, $e_j(k+1) \approx e_j(k)$.

[24], [35] indicate that a one-step delay issue exists in this method, and [36] proposes the two-step prediction to compensate the time delay:

$$\begin{cases} i_\alpha(k+2) = \frac{T_s\left[u_\alpha(k+1) - e_\alpha(k+1) - \left(1-\frac{T_s}{L}\right)i_\alpha(k+1)\right]}{L} \\ i_\beta(k+2) = \frac{T_s\left[u_\beta(k+1) - e_\beta(k+1) - \left(1-\frac{T_s}{L}\right)i_\beta(k+1)\right]}{L} \end{cases} \quad (13)$$

where $i_\alpha(k+2)$ and $i_\beta(k+2)$ are the two-step predictive values serving as references for the current loop; and $u_\alpha(k+1)$ and $u_\beta(k+1)$ are the predictive values at the $(k+1)th$ instant, which can be used to calculate the reference for the vector selection.

The predictive equations are a basic description of the system, the designed cost function is used to evaluate their performance. Therefore, this is the essential part to be discussed. The cost function consists of two parts: g_1 is used to reflect the effects of the output voltage, and g_2 is used to reflect the performance of the NP current regulation.

$$g = g_1 + g_2 \quad (14)$$

$$g_1 = (u_{\alpha ref} - u_\alpha(k+1))^2 + (u_{\beta ref} - u_\beta(k+2))^2 \quad (15)$$

$$g_2 = f(\Delta V_{NP}, i_{sv1}, i_{sv2}, i_{mv}, t_{sv1}, t_{sv2}, t_{mv}, k_1) \quad (16)$$

It can be seen from equation (16) that g_2 is a function of the capacitor voltage difference ΔV_{NP}, the small vector coefficient k_1, the NP current of each vector i_j, and the dwelling time of each vector t_j, where $(j = sv1, sv2, mv)$.

To avoid a non-constant switching frequency, the vectors are appropriately arranged [30], [37]. Once the vectors $u_i(i = 1,2,3)$ are selected, the corresponding dwelling times $t_i(i = 1,2,3)$ are decided. Two-step predictions in the discrete time model are:

$$\begin{cases} u_\alpha^{k+1} = u_\alpha^k + \sum_{i=1}^3 c_{\alpha i} t_i \\ u_\beta^{k+1} = u_\beta^k + \sum_{i=1}^3 c_{\beta i} t_i \\ \sum_{i=1}^3 t_i = T_s \end{cases} \quad (17)$$

where u_α^{k+1} and u_β^{k+1} are the predictive values for the $(k+1)th$ sampling instant; u_α^k and u_β^k are the initial values at the kth instant; $c_{\alpha i}$ and $c_{\beta i}$ are the increments for the selected vector u_i in the $\alpha\beta$ axes; and t_i represents the corresponding time of each vector.

In the FCS-MPC, the final goal of the optimal search is to select elements with the minimum cost function value. In this part, three vectors surrounding the reference vector are selected in one switching period. The vectors lead to the minimum g_1. Thus, their dwelling times have to satisfy (18):

$$\begin{cases} \frac{\partial g_1}{\partial t_1} = 0 \\ \frac{\partial g_1}{\partial t_2} = 0 \\ t_3 = T_s - t_1 - t_2 \end{cases} \quad (18)$$

$$\begin{cases} t_1 = \frac{\begin{matrix}(u_{\alpha ref} - u_\alpha^k - T_s c_{\alpha 3})(c_{\beta 2} - c_{\beta 3}) \\ -(u_{\beta ref} - u_\beta^k - T_s c_{\beta 3})(c_{\alpha 2} - c_{\alpha 3})\end{matrix}}{(c_{\alpha 1} - c_{\alpha 3})(c_{\beta 2} - c_{\beta 3}) - (c_{\beta 1} - c_{\beta 3})(c_{\alpha 2} - c_{\alpha 3})} \\ t_1 = \frac{\begin{matrix}(u_{\beta ref} - u_\beta^k - T_s c_{\beta 3})(c_{\alpha 1} - c_{\alpha 3}) \\ -(u_{\alpha ref} - u_\alpha^k - T_s c_{\alpha 3})(c_{\beta 1} - c_{\beta 3})\end{matrix}}{(c_{\alpha 1} - c_{\alpha 3})(c_{\beta 2} - c_{\beta 3}) - (c_{\beta 1} - c_{\beta 3})(c_{\alpha 2} - c_{\alpha 3})} \\ t_3 = T_s - t_1 - t_2 \end{cases} \quad (19)$$

With this method, the effects of the time delay in this system are alleviated.

B. The Multistage Medium Vector Method

As mentioned before, the medium vector is the object to be modified. The analysis previously presented indicates that the control of medium vectors is the key to fixing these issues. Therefore, the modified medium voltage vectors, which consist of virtual medium vectors and the original medium vectors, are utilized in this strategy. The proposed novel vector is the multilevel medium vector (MMV), which has a variable magnitude:

$$\begin{cases} |\vec{V}_{m\_novel}| = kv|\vec{V}_{cmv}| + (1-kv)|\vec{V}_m| \\ \vec{V}_{obj}T_s = \vec{V}_{m\_novel}t_m + \vec{V}_{sv1}t_1 + \vec{V}_{sv2}t_2 \end{cases} \quad (20)$$

where $\vec{V}_{cmv}$ is the conventional virtual medium vector; $\vec{V}_m$ is the original medium vector; $\vec{V}_{m\_novel}$ is the MMV; kv $(0 \le kv \le 1)$ is the coefficient denoting the proportion of the virtual one in $\vec{V}_{m\_novel}$; and t_1, t_2 and t_m are the dwelling times for $\vec{V}_{sv1}$, $\vec{V}_{sv2}$ and $\vec{V}_{m\_novel}$, respectively.

Since the medium vector is neither the absolutely original medium vector nor the absolutely virtual medium one, it can inject the NP current into the NP node according to the conditions of the system.

Unlike the conventional FCS-MPC, kv is used as an element for an optimal search in this algorithm. Based on the

form of the FCS-MPC, kv is transformed to the discrete value $kv(i)$. It can be concluded from equation (20) that $0 \le kv \le 1$. Take the extreme cases into consideration: a) $kv(i) = 1$, this method is equivalent to the CVV-SVM method; and b) $kv(i) = 0$, this method is equivalent to the CSVM method. In another words, the value of $kv(i)$ denotes the modulation pattern switch.

Thus, the proposed algorithm can be regarded as an improved virtual vector method. Under the assumption that i_{sv1} is used to regulate the NPP and k_1 is its coefficient, the detailed expression of g_2 is:

$$g_2 = \left| -C * \Delta V_{NP} - \left(1 - kv(i)\right) t_{mv} i_{mv} - (1 - 2k_1) i_{sv1} t_{sv1} - i_{sv2} t_{sv2} \right| \quad (21)$$

The sub-sectors in one sector are also re-divided to cooperate with the MMV. Take sector III as an example, the novel sub-sectors are illustrated in Fig. 4. Unlike Fig. 3, the area of each sub-sector is not constant. The dashed lines of the same color make up the boundaries of the new sub-sectors. According to the different values of $kv(i)$, the area of each sector varies.

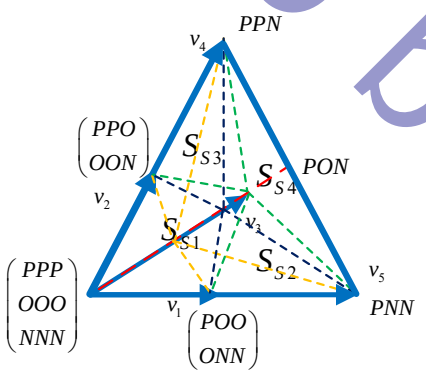

Fig. 4. MMV in Sector III.

As can be seen in Fig. 4, one sector consists of four parts. Based on the proposed method, the virtual medium vector and the original one both participate in the synthesis of the reference vector in each sub-sector. The sequence arrangement of the vectors in one sampling period is introduced as follows.

1) Sub-Sector S_{S1}

Sub-sector S_{S1} is a quadrilateral part in Fig. 4.

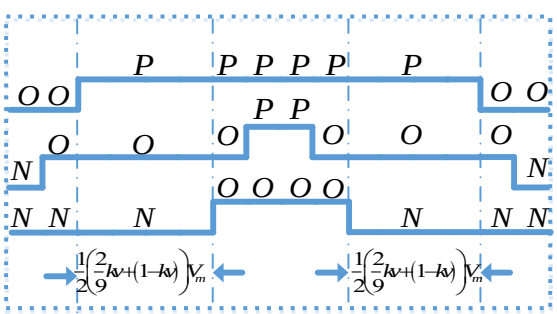

Fig. 5. Vector Sequence of S_1.

The detailed steps are shown as follows.

a) The initial value of $kv(i)$ is set to zero. Calculate the time of each vector with equations (6), (12), (13), (15) and (19).
b) Calculate k_1 in equation (21), and evaluate the result of g_2. If k_1 is suitable for the system, meaning that $|g_2| < \varepsilon$ $(\varepsilon \ge 0)$, the value of $kv(i)$ and k_1 is applied to implement the control.
c) If k_1 is not suitable for the system, choose the next value of $kv(i)$. Then repeat step (1) and step (2). Evaluate g_2 for the new $kv(i)$ and store their values.
d) If the result from step (3) is suitable for the system, apply it to implement the control. If it does not work, repeat step (3). If all of the results are not suitable, select the value of $kv(i)$ which offers the minimum g_2.

In this paper, the original medium vector is divided into equivalent proportions, and each part is equal to 1/N (N=1,2,3,4…) of the original one. The regulation of $kv(i)$ is add 1/N to the former value until $kv(i) = 1$.

Assume that all five vectors are used. The switching sequence is displayed in Fig. 5. Consider the least switching process and symmetric pulses, which are preferred in the modulation [3]. The sequence of the selected voltage vectors is ONN-OON-PON-POO-PPO.

2) Sub-Sector S_{S2}

In this sub-sector, the NP current is the sum of i_a and i_b. The sequence of the employed voltage vectors is PPO-POO-PON-PNN-ONN.

3) Sub-Sector S_{S3}

In this sector, the sequence of the employed voltage vectors is PPO-PPN-PON-OON-ONN.

4) Sub-Sector S_{S4}

In this sector, the sequence of the employed voltage vectors is PPO-PPN-PON-PNN-ONN. Since the medium vector in this sector is the only one that generates the NP current, manipulating the medium vector directly regulates the NPP. In other words, when the MI is high, the MMV method can still adjust the NPP, which exceeds the CVV-SVM method in this regard.

As previously mentioned, the cost function is $g(f) = g_1 + g_2$. With a comparison of $g(f)$ in different $kv(i)$, the optimal vectors are selected.

IV. Simulation and Experimental Results

A. Simulation Results

To verify the validity of the proposed algorithm, a simulation model of the system is constructed in MATLAB. Simulation and the experimental results of the proposed algorithm, the CSVM method and the CVV-SVM method are presented in this section. The parameters of the system are displayed in Table II.

In this paper, the MI is defined as follows:

$$m = \frac{U_r}{\sqrt{3}U_{dc}} \quad (22)$$

where m is the MI, U_r is the peak value of the output phase voltage, and U_{dc} is the value of the dc voltage.

TABLE II
PARAMETERS OF THE SYSTEM

L	$6\,mH$
C_1	$500\,\mu F$
C_2	$1000\,\mu F$
DC Voltage	$100V$
Modulation Index	≤0.9
Switching Frequency	5kHz

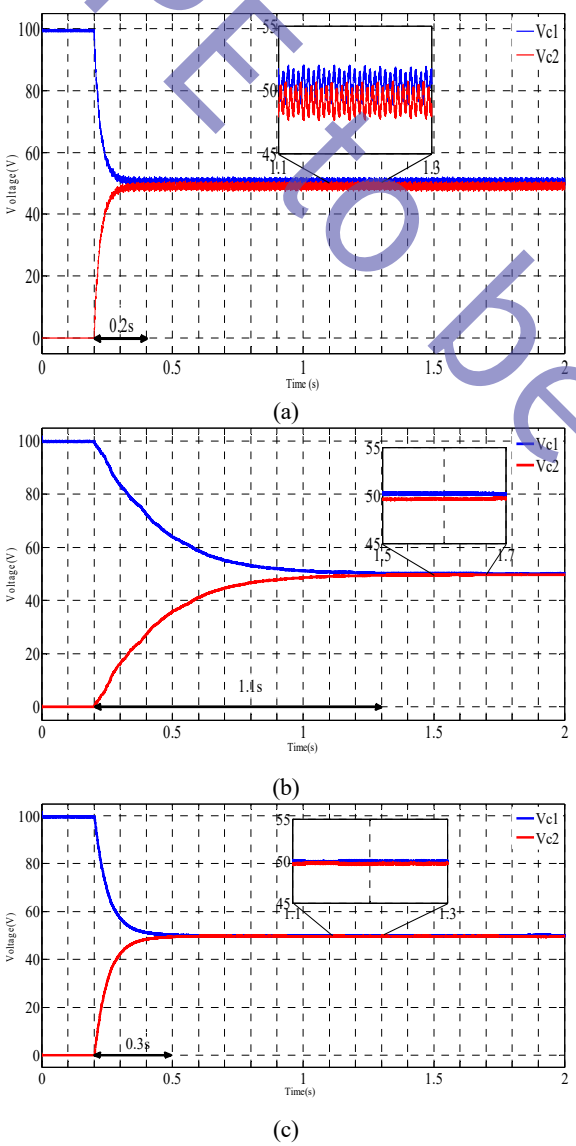

Fig. 6. Simulation results of the balancing process of the three methods. (a) Balancing process of the CSVM. (b) Balancing process of the CVV-SVM. (c) Balancing process of the MMV.

In this section, the CSVM and the CVV-SVM methods utilize a PI controller to implement the voltage loop and the current loop, while the proposed MMV uses the FCS-MPC algorithm. Fig. 6 illustrates the balancing process of the three methods.

Considering extreme conditions, the load of the system is purely resistive, 10Ω in each phase. The initial voltage of the upper capacitor C_1 is 100V, and the voltage of C_2 is 0V. The NPP regulation starts to work at 0.2s.

As mentioned before, the proposed method can be regarded as a hybrid of the two conventional methods. To distinguish them, the value of $kv(i)$ excludes 0 and 1.

It can be seen from Fig. 6 that without the virtual vector the CSVM needs the least time to finish the regulation of the drifted NPP, while the proposed method needs 0.3s, which is longer than the CSVM method. The CVV-SVM method needs almost 1.1s to finish this process, which is the longest. However, in the steady state, the amplitude of the NPP oscillation in the CSVM method is the largest. In the CVV-SVM and the proposed method, the oscillation of the NPP is eliminated. However, in the steady state, the drifted NPP still exists in the CVV-SVM.

B. Experimental Results

To validate the proposed algorithm, experiments have been implemented on a prototype of a 1KVA three-level NPC converter in lab. Fig. 7 displays the hardware of the control part of the converter.

The IGBT is an Infineon FS3L30R07W2H3F, the microcontroller is a TI DSP TMS320C6748 and a Xilinx Spartan 6E. The parameters of the system are the same as those in Table II. The dead time of the IGBT is set to 4μs.

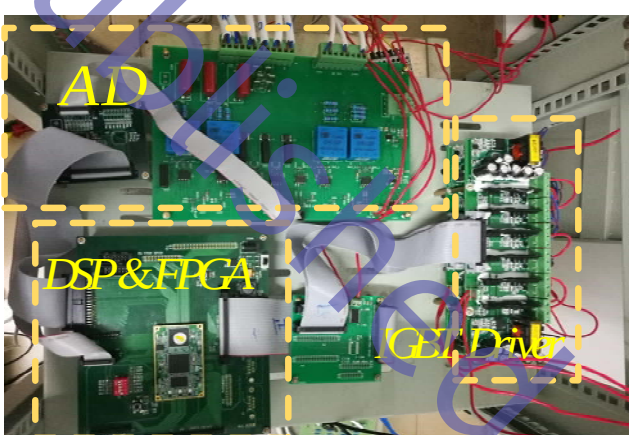

Fig. 7. Experimental platform.

Since the NPP oscillation elimination is the essential target in this paper, only the CVV-SVM and the MMV are compared in these experiments.

Fig. 8 displays the balancing process of the NPP in different modulation indexes.

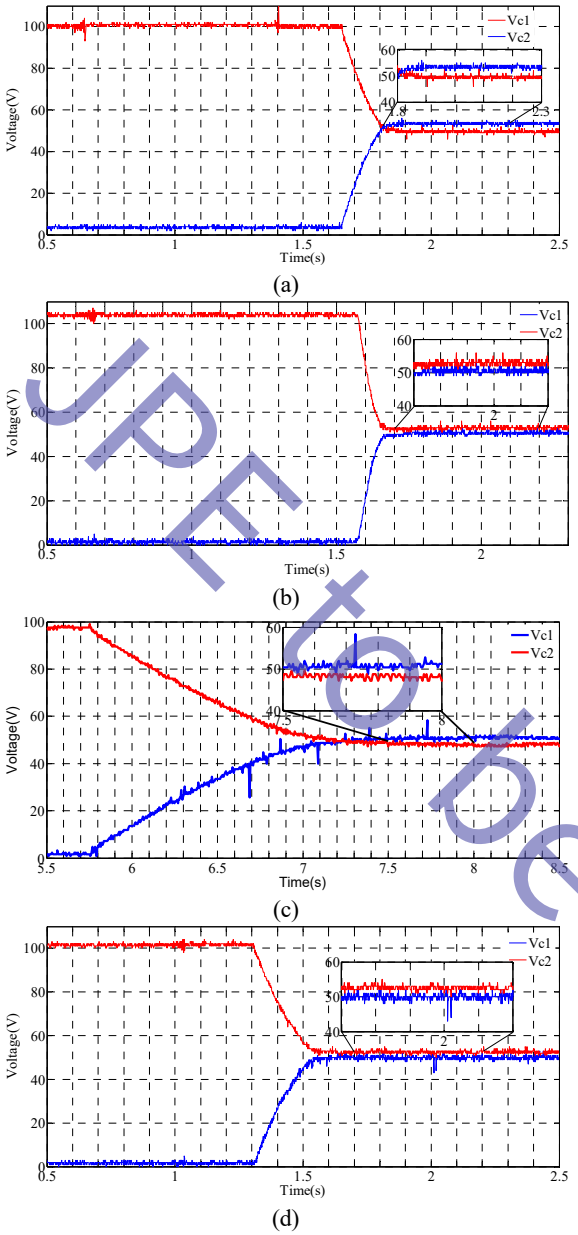

Fig. 8. Experimental results of the balancing process. (a) Balancing process of the CVV-SVM, m=0.7. (b) Balancing process of the MMV, m=0.7. (c) Balancing process of the CVV-SVM, m=0.9.

Fig. 8 displays a comparison of the CVV-SVM and the MMV method during the balancing process. As can be seen, although the dc-link capacitors are not identical, both methods can fix the drifted NPP. Moreover, the oscillations of the NPP are eliminated.

Fig. 8(a) and Fig. 8(b) display their transient process when m=0.7. Since the MI is moderate, the small vectors in the CVV-SVM can be used to regulate the NPP. The CVV-SVM method needs 0.15s to fix the drifted NPP and the MMV method needs 0.1s. Moreover, a slight difference between the two capacitors exists in the CVV-SVM.

Accompany by an increase of the MI, the balancing process is prolonged as analysed in Section III. Fig. 8(c) and Fig. 8(d), which show their processes when m=0.9, reveal the same conclusion as the analysis. The CVV-SVM method needs 1.5s to fix the drifted NPP. Moreover, the difference between the two capacitors still exists in the steady state. On the other hand, the MMV method can still regulate the voltage of the capacitors. The time of the balancing process is almost 0.3s. The MMV participates in the regulation of the NPP, and the dynamic performance is improved.

As previously mentioned, the reduced calculation time is another merit of the proposed algorithm when compared with the conventional FCS-MPC. Using the output of a DSP as the indicator reveals the calculation time of the vector selection.

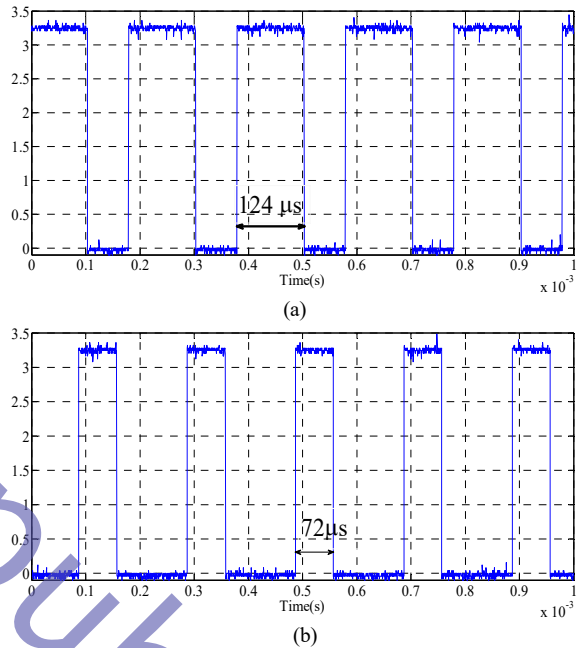

Fig. 9. Vector selection time. (a) Vector selection time for the conventional FCS-MPC. (b) Vector selection time for the MMV.

The high-level output state denotes the time that the vector selection lasts. From Fig. 9(a) it can be seen that the vector selection process lasts 124 µs. Meanwhile in Fig. 9(b), the time is 72 µs. Since the optimal vector search is limited in one sector, the time consumption is reduced.

When m=0.8, the current of phase A and the switching state of V_{ab} in the steady state are displayed in Fig. 10.

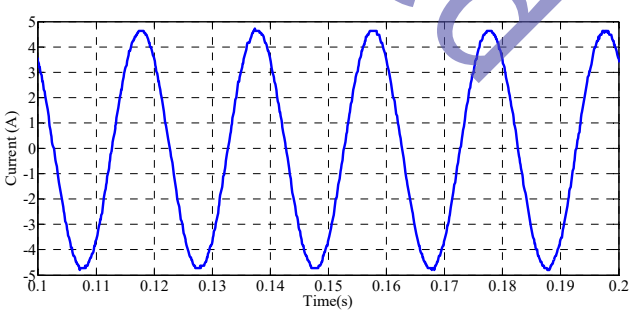

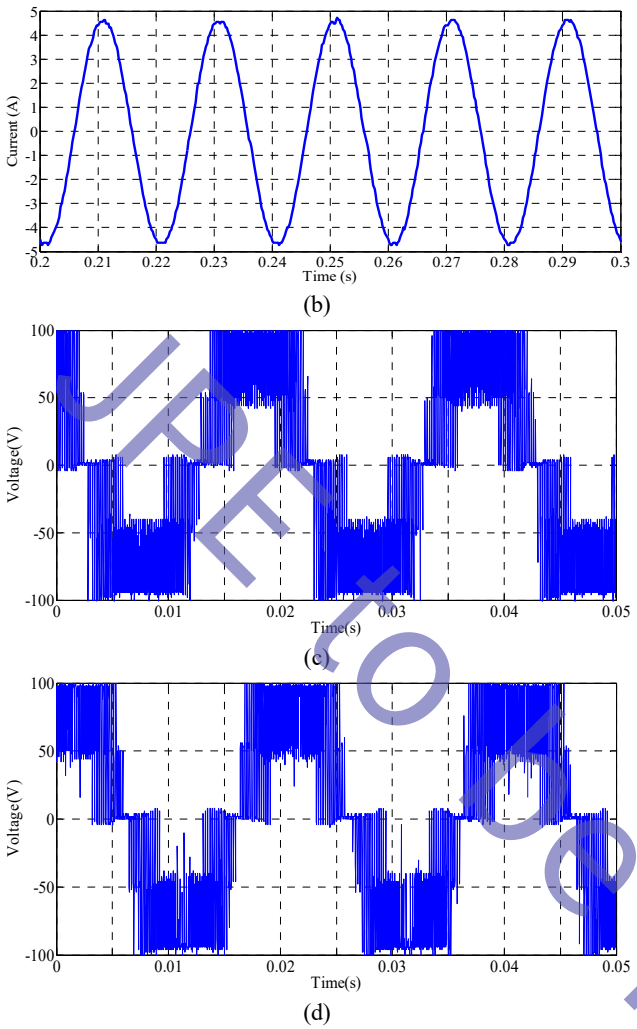

Fig. 10. Experimental results of current and switching waveform. (a) Current of phase A in the CVV-SVM. (b) Current of phase A in the MMV. (c) Switching waveform of the CVV-SVM. (d) Switching waveform of the MMV.

To compare the output current performance of the CVV and the MMV, the phase current of each algorithm shown in Fig. 10 is dealt with a FFT in MATLAB, and the results are shown in Fig. 11.

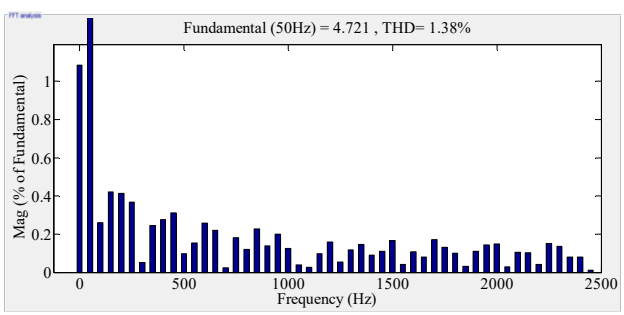

(a)

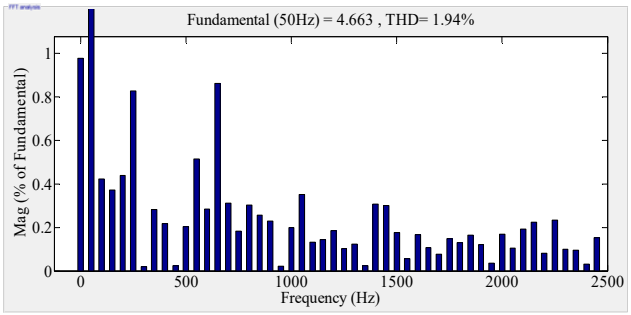

(b)

Fig. 11. FFT of experimental current A. (a) FFT of current A in the CVV. (b) FFT of current A in the MMV.

It can be seen from Fig. 11 that the THD of the CVV-SVM is 1.38%, and the THD of the MMV is 1.94%. In addition, both of them are far less than 5%. The proposed method does not significantly increase the THD of the output current.

V. Conclusion

This paper proposes a multistage medium vector method that combines the FCS-MPC to resolve the NPP oscillation and the drifted NPP of 3L-NPC inverters. The proposed algorithm provides adjustable magnitude medium voltage vectors. To cooperate with the novel vector, re-divisions of the sub-sectors and the arrangements of the voltage vectors are provided.

Simulation and experimental results verify that in addition to the mitigation of the NPP oscillation, the ability to fix the drifted NPP in the proposed algorithm is less sensitive to the modulation index. This reduces the size of the system and improves the reliability of three-level NPC converters.

References

[1] G. I. Orfanoudakis, M. A. Yuratich, and S. M. Sharkh, "Nearest-vector modulation strategies with minimum amplitude of low-frequency neutral-point voltage oscillations for the neutral-point-clamped converter," *IEEE Trans. Power Electron.*, Vol. 28, No. 10, pp. 4485-4499, Oct. 2013.

[2] R. Raushan, B. Mahato, and K. C. Jana, "Comprehensive analysis of a novel three-phase multilevel inverter with minimum number of switches," *IET Power Electron.*, Vol. 9, No. 8, pp. 1600-1607, Jun. 2016.

[3] M. Ke and F. Blaabjerg, "Modulation methods for three-level neutral-point-clamped inverter achieving stress redistribution under moderate modulation index," *IEEE Trans. Power Electron.*, Vol. 31, No. 1, pp. 5-10, Jan. 2016.

[4] J. Lyu, W. Hu, F. Wu, K. Yao, and J. Wu, "Variable modulation offset SPWM control to balance the neutral-point voltage for three-level inverters," *IEEE Trans. Power Electron.*, Vol. 30, No. 12, pp. 7181-7192, Dec. 2015.

[5] U.-M. Choi, F. Blaabjerg, and K.-B. Lee, "Method to Minimize the Low-Frequency Neutral-Point Voltage oscillations with time-offset injection for neutral-point-clamped inverters," *IEEE Trans. Ind. Appl.*, Vol. 51, No. 2, pp. 1678-1691, Mar./Apr. 2015.

[6] I. Lopez, S. Ceballos, J. Pou, J. Zaragoza, J. Andreu, I.

Kortabarria, and V. G. Agelidis "Modulation strategy for multiphase neutral-point-clamped converters," *IEEE Trans. Power Electron.*, Vol. 31, No. 2, pp. 928-941, Feb. 2016.

[7] J. Lee and K. Lee, "Time-offset injection method for neutral-point AC ripple voltage reduction in a three-level inverter," *IEEE Trans. Power Electron.*, Vol. 31, No. 3, pp. 1931-1941, Mar. 2016.

[8] C. Wang and Y. Li, "Analysis and calculation of zero-sequence voltage considering neutral-point potential balancing in three-level NPC converters," *IEEE Trans. Ind. Electron.*, Vol. 57, No. 7, pp. 2262-2271, Jul. 2010.

[9] W. D. Jiang, S. W. Du, L. C. Chang, Y. Zhang, and Q. Zhao, "Hybrid PWM strategy of SVPWM and VSVPWM for NPC three-level voltage-source inverter," *IEEE Trans. Power Electron.*, Vol. 25, No. 10, pp. 2607-2619, Oct. 2010.

[10] J. Pou, J. Zaragoza, S. Ceballos, M. Saeedifard, and D. Boroyevich, "A carrier-based PWM strategy with zero-sequence voltage injection for a three-level neutral-point-clamped converter," *IEEE Trans. Power Electron.*, Vol. 27, No. 2, pp. 642-651, Feb. 2012.

[11] R. Maheshwari, S. Munk-Nielsen, and S. Busquets-Monge, "Design of neutral-point voltage controller of a three-level NPC inverter with small DC-link capacitors," *IEEE Trans. Ind. Electron.*, Vol. 60, No. 5, pp. 1861-1871, May 2013.

[12] A. A. M. Bento, K. V. D. d. Almeida, J. A. R. M. Oliveira, E. R. C. d. Silva, and C. B. Jacobina, "A high power factor three-phase three-level rectifier," in *2007 IEEE Power Electronics Specialists Conference*, pp. 3040-3045, Jun. 2007.

[13] J. Zaragoza, J. Pou, S. Ceballos, E. Robles, C. Jaen, and M. Corbalan, "Voltage-balance compensator for a carrier-based modulation in the neutral-point-clamped converter," *IEEE Trans. Ind. Electron.*, Vol. 56, No. 2, pp. 305-314, Feb. 2009.

[14] S. Wensheng, F. Xiaoyun, and K. M. Smedley, "A carrier-based PWM strategy with the offset voltage injection for single-phase three-level neutral-point-clamped converters," *IEEE Trans. Power Electron.*, Vol. 28, No. 3, pp. 1083-1095, Mar. 2013.

[15] H. Akagi and T. Hatada, "Voltage balancing control for a three-level diode-clamped converter in a medium-voltage transformerless hybrid active filter," *IEEE Trans. Power Electron.*, Vol. 24, No. 3, pp. 571-579, Mar. 2009.

[16] U.-M. Choi, J.-S. Lee, and K.-B. Lee, "New modulation strategy to balance the neutral-point voltage for three-level neutral-clamped inverter systems," *IEEE Trans. Energy Convers.*, Vol. 29, No. 1, pp. 91-100, Mar. 2014.

[17] A. Bendre, S. Krstic, J. Vander Meer, and G. Venkataramanan, "Comparative evaluation of modulation algorithms for neutral-point-clamped converters," *IEEE Trans. Ind. Appl.*, Vol. 41, No. 2, pp. 634-643, Mar./Apr. 2005.

[18] S. Jie, S. Schroder, B. Duro, and R. Roesner, "A neutral-point balancing controller for a three-level inverter with full power-factor range and low distortion," *IEEE Trans. Ind. Appl.*, Vol. 49, No. 1, pp. 138-148, Jan./Feb. 2013.

[19] P. Chaturvedi, S. Jain, and P. Agarwal, "Carrier-based neutral point potential regulator with reduced switching losses for three-level diode-clamped inverter," *IEEE Trans. Ind. Electron.*, Vol. 61, No. 2, pp. 613-624, Jan./Feb. 2014.

[20] S. Busquets-Monge, J. Bordonau, D. Boroyevich, and S. Somavilla, "The nearest three virtual space vector PWM - a modulation for the comprehensive neutral-point balancing in the three-level NPC inverter," *IEEE Power Electron. Lett.*, Vol. 2, No. 1, pp. 11-15, Mar. 2004.

[21] C. Xia, H. Shao, Y. Zhang, and X. He, "Adjustable proportional hybrid SVPWM strategy for neutral-point-clamped three-level inverters," *IEEE Trans. Ind. Electron.*, Vol. 60, No. 10, pp. 4234-4242, Oct. 2013.

[22] S. Calligaro, F. Pasut, R. Petrella, and A. Pevere, "Modulation techniques for three-phase three-level NPC inverters: A review and a novel solution for switching losses reduction and optimal neutral-point balancing in photovoltaic applications," in *Applied Power Electronics Conference and Exposition (APEC), 2013 Twenty-Eighth Annual IEEE*, pp. 2997-3004, May 2013.

[23] M. Narimani, B. Wu, V. Yaramasu, and N. Reza Zargari, "Finite control-set model predictive control (FCS-MPC) of nested neutral point-clamped (NNPC) converter," *IEEE Trans. Power Electron.*, Vol. 30, No. 12, pp. 7262-7269, Jan. 2015.

[24] D.-K. Choi and K.-B. Lee, "Dynamic performance improvement of AC/DC converter using model predictive direct power control with finite control set," *IEEE Trans. Ind. Electron.*, Vol. 62, No. 2, pp. 757-767, Feb. 2015.

[25] V. Yaramasu, M. Rivera, M. Narimani, W. Bin, and J. Rodriguez, "Model predictive approach for a simple and effective load voltage control of four-leg inverter with an output LC filter," *IEEE Trans. Ind. Electron.*, Vol. 61, No. 10, pp. 5259-5270, Oct. 2014.

[26] P. Karamanakos, T. Geyer, N. Oikonomou, F. D. Kieferndorf, and S. Manias, "Direct model predictive control: A review of strategies that achieve long prediction intervals for power electronics," *IEEE Ind. Electron. Mag.*, Vol. 8, No. 1, pp. 32-43, Mar. 2014.

[27] Z. Song, C. Xia and T. Liu, "Predictive current control of three-phase grid-connected converters with constant switching frequency for wind energy systems," *IEEE Trans. Ind. Electron.*, Vol. 60, No. 6, pp. 2451-2464, Jun. 2013.

[28] S. Kwak and J.-C. Park, "Switching strategy based on model predictive control of VSI to obtain high efficiency and balanced loss distribution," *IEEE Trans. Power Electron.*, Vol. 29, No. 9, pp. 4551-4567, Sep. 2014.

[29] R. O. Ramirez, J. R. Espinoza, F. Villarroel, E. Maurelia, and M. E. Reyes, "A novel hybrid finite control set model predictive control scheme with reduced switching," *IEEE Trans. Ind. Electron.*, Vol. 61, No. 11, pp. 5912-5920, Nov. 2014.

[30] S. Vazquez, A. Marquez, R. Aguilera, D. Quevedo, J. I. Leon, and L. G. Franquelo, "Predictive optimal switching sequence direct power control for grid-connected power converters," *IEEE Trans. Ind. Electron.*, Vol. 62, No. 4, pp. 2010-2020, Apr. 2015.

[31] A. Calle-Prado, S. Alepuz, J. Bordonau, J. Nicolas-Apruzzese, P. Cortes, and J. Rodriguez, "Model predictive current control of grid-connected neutral-point-clamped converters to meet low-voltage ride-through requirements," *IEEE Trans. Ind. Electron.*, Vol. 62, No. 3, pp. 1503-1514, Mar. 2015.

[32] A. Nabae, I. Takahashi, and H. Akagi, "A new neutral-point-clamped PWM inverter," *IEEE Trans. Ind. Appl.*, Vol. IA-17, No. 5, pp. 518-523, Sep. 1981.

[33] J. Pou, R. Pindado, D. Boroyevich, and P. Rodriguez, "Evaluation of the low-frequency neutral-point voltage oscillations in the three-level inverter," *IEEE Trans. Ind. Electron.*, Vol. 52, No. 6, pp. 1582-1588, Dec. 2005.

[34] H. Fang, Z. Zhang, X. Feng, and R. Kennel, "Ripple-reduced model predictive direct power control for active front-end power converters with extended switching vectors and time-optimised control," *IET Power Electron.*, Vol. 9, No. 9,

pp. 1914-1923, Jul. 2016.
[35] S. Aurtenechea, M. A. Rodriguez, E. Oyarbide, and J. R. Torrealday, "Predictive direct power control – A new control strategy for DC/AC converters," in *IECON 2006 - 32nd Annual Conference on IEEE Industrial Electronics*, pp. 1661-1666, Nov. 2006.
[36] S. Kwak and S. Mun, "Common-mode voltage mitigation with a predictive control method considering dead time effects of three-phase voltage source inverters," *IET Power Electron*., Vol. 8, No. 9, pp. 1690-1700, Sep. 2015.
[37] L. Tarisciotti, P. Zanchetta, A. Watson, J. C. Clare, M. Degano, and S. Bifaretti, "Modulated model predictive control for a three-phase active rectifier," *IEEE Trans. Ind. Appl*., Vol. 51, No. 2, pp. 1610-1620, Mar. 2015.

Yuan Yao was born in Liaoning province, China, in 1990. He received his B.S. and M.S. degrees in Electrical Engineering from Dalian Maritime University, Dalian, China, in 2012 and 2014, respectively. He is presently working towards his Ph.D. degree in Power Electronics and Power Drives from the School of Electric Power, South China University of Technology, Guangzhou, China. His current research interests include pulse width modulation converter/inverter systems, multilevel conversion and ac power conversion applied to renewable energy systems.

Longyun Kang was born in Jilin, China, in 1961. He received his B.S. degree in Physics from Yanbian University, Yanji, China, in 1982; and his M.S. and Ph.D. degrees in Electrical Engineering from the Department of Engineering of Kyoto University, Kyoto, Japan, in 1996 and 1999, respectively. From 1999 to 2001, he was a Researcher in the Department of Engineering, Tokyo Institute of Technology, Tokyo, Japan. From 2001 to 2006, he was an Associate Professor in the Institute of Mechanical Engineering, Xi'an Jiaotong University, Xi'an, China. Since 2006, he has been with the School of Electric Power, South China University of Technology, Guangzhou, China, where he is presently working as a Professor. He supervises six Ph.D. students and serves as a Director of the Guangdong Key Laboratory of Clean Energy Technology. His current research interests include renewable energy and electric vehicles, including wind energy, solar energy conversion, hybrid energy systems, and hybrid-drive technology of electric vehicles.

Zhi Zhang was born in Hunan province, China. He received his B.S. degree in Automation from Xiangtan University, Xiangtan, China, in 2003; his M.S. degree in Power Electronics and Power Drives from Guangxi University, Nanning, China, in 2007; and his Ph.D. degree in Power Electronics and Power Drives from the South China University of Technology, Guangzhou, China, in 2010. He is presently working as a Senior Engineer in the Department of Electrical Engineering, Dongguan University of Technology, Dongguan, China. His current research interests include power electronics, electrical machines, new renewable energy, and UPS systems.